NRIAG Journal of Astronomy and Geophysics (2013) **2**, 125–133

National Research Institute of Astronomy and Geophysics

NRIAG Journal of Astronomy and Geophysics

www.elsevier.com/locate/nrjag

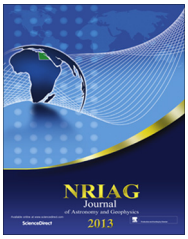

Theoretical infrared continuum images for Be star disks

Gamal Edin Hamed *, T.A.A. Sigut

National Research Institute of Astronomy and Geophysics, Helwan, Cairo, Egypt
University of Western Ontario, London, Ontario N6A 3K7, Canada

Received 30 October 2012; accepted 29 April 2013
Available online 30 June 2013

Abstract We present theoretical infrared images for Be star disks as projected on the plane of the sky. These images span a range of Be star spectral types and a wide range of disk properties and viewing inclinations. We extract the sizes of these disks at different IR wavelengths. As a test of these images, we compare our calculated disk sizes with available interferometric observations of the Be stars α Ara and ζ Tau. We use our calculated disk sizes and the observations to constrain the disk parameters of these stars.

1. Introduction

1.1. Be stars

Classical Be stars are non-supergiant B stars which have shown one or more Balmer emission lines over the time period during which they have been observed. Be stars are believed to rotate close to the critical velocity at which their equatorial velocity equals the orbital speed. However, recent studies suggest that they may in fact not be critically rotating (Cranmer, 2005). The first star to be identified as a Be star was γ Cas in 1866 when Angelo Secchi noticed a Balmer emission line in its spectrum instead of an absorption line (Porter and Rivinius, 2003). These emission lines are believed to be due to the presence of an equatorial disk around the star formed via outflow of photospheric gas. However the mechanism of disk formation is still unknown (Porter and Rivinius, 2003). There is good evidence that Be star disks are supported by Keplerian rotation (Hummel and Vrancken, 2000), and this was confirmed for α Ara by interferometric observations (Meilland et al., 2007).

Zorec and Briot (1997) made a statistical study of the frequency of Be stars among main sequence B stars taking into account many uncertainties that might affect the count of Be stars. They found that, overall, 17% of non-supergiant B type stars are Be stars. However, this frequency varies widely with the spectral type, from 27% for B0, the hottest spectral subclass, to only 8% for B9, the coolest spectral subclass. The maximum frequency is 34% for B1 stars. It also seems that low metallicity clusters have a higher frequency of Be stars, suggesting that metallicity affects the occurrence of a disk (Maeder et al., 1999).

* Corresponding author at: National Research Institute of Astronomy and Geophysics, Helwan, Cairo, Egypt. Mobile: +20 116997507.
E-mail address: ghamed@alumni.uwo.ca (G. Hamed).
Peer review under responsibility of National Research Institute of Astronomy and Geophysics.

Production and hosting by Elsevier

2090-9977 © 2013 Production and hosting by Elsevier B.V. on behalf of National Research Institute of Astronomy and Geophysics.
http://dx.doi.org/10.1016/j.nrjag.2013.06.015

The density of the disk is often assumed to have a power-law dependence on the radius as $\rho \propto r^{-n}$ (Waters, 1986). Some models consider density to be decreasing exponentially in the perpendicular direction (for example Marlborough, 1969; Poeckert and Marlborough, 1978), and these models are based on the assumption that the disks are in vertical hydrostatic equilibrium. The value of the power-law index n has been constrained to be between 2 and 4 by modeling the observed IR spectral energy distributions of Be stars from IRAS, while radio continuum observations suggest values for n higher than 4. This can be explained by flaring or cooling of the disk in outer regions (Taylor et al., 1987).

1.2. IR disk emission

Be stars show excess in IR radiation relative to that expected from the central B star alone. This excess is due to the free–free and free–bound emission from the circumstellar disk (Woolf et al., 1970; Gehrz et al., 1974; Waters, 1986).

Electron scattering of photospheric light is the main contribution to the disk's emission in the optical region of the continuum.

2. Observed IR excess

To quantitatively predict the IR excess of Be stars, Waters (1986) developed a formula for the optical depth of the disk along the line of sight,

$$\tau_v(q) = E_{\rm vd} \int x^{-2n+1}(x^2 - q^2)^{-1/2} dx, \tag{1}$$

where q is the impact parameter (which is the perpendicular distance from the line of sight to the center of the star in units of R_*), and $E_{\rm vd}$ is an optical depth parameter defined by

$$E_{\rm vd} = X_\lambda X_{*_d}, \tag{2}$$

where

$$X_\lambda = \lambda^2 \frac{(1 - e^{-h\nu/KT})}{(h\nu/KT)} (g(\nu, T) + b(\nu, T)) \tag{3}$$

and

$$X_{*_d} = 4.923 \times 10^{35} \overline{z^2} T^{-3/2} \mu^{-2} \gamma \rho^2 R_* \tag{4}$$

Table 1 Stellar parameters of α Ara and ζ Tau.

Star	α Ara	ζ Tau
Spectral Type	B3V[c]	B3V
V (mag)	2.9[b]	3.00[a]
Effective temperature (K)	18044[c]	19340[c]
Mass ($M_\odot$)	9.6[b]	11.2[d]
Luminosity ($L_\odot$)	2200[b]	7400[e]
Radius ($R_\odot$)	4.8[b]	5.5[d]
Distance (pc)	81[c]	136[c]

References:
[a] Quirrenbach et al. (1997).
[b] Chesneau et al. (2005).
[c] Meilland et al. (2009).
[d] Gies et al. (2007).
[e] Carciofi et al. (2009).

Here λ is the wavelength in cm, ν is the frequency in Hz, $g(\nu, T)$ is the free–free Gaunt factor, $b(\nu, T)$ is the free–bound Gaunt factor, z^2 is the mean value of the square of the atomic charge, γ is the ratio between the numbers of electrons and ions, μ is the mean atomic weight in proton mass units, R_* is the stellar radius in R_*, T is the temperature in K, and ρ_o is the disk base density. From the previous equations, we can see the dependence of the optical depth of the disk on the square of the wavelength, and this explains the apparent increase in the size of the disk and excess flux with the increasing wavelength. The disk optical depth is also strongly affected by the disk base density (ρ_o) and the ionization state of the disk gas (γ). We shall directly demonstrate these effects in Section 5.

3. Near IR images of Be stars

3.1. Interferometric studies

Optical interferometry results from the coherent combination of visible or IR light collected by several telescopes. Due to the atmospheric turbulence, the diffraction limit of large, single, ground-based telescopes is never achieved, and all stars remain unresolved point sources. We can obtain much better angular resolution by using interferometers with large baselines. In the case of optical interferometry, the angular resolution is set by λ/B where λ is the observing wavelength and B is the baseline, which is the distance between the telescopes (Schöller, 2003).

An interferometer measures the complex visibility defined as

$$V(f_y, f_z, \lambda) \equiv |v(f_y, f_{z,,\lambda})| e^{i\varphi(f_y, f_z, \lambda)} \tag{5}$$

$$= \frac{\widetilde{I}_\lambda(f_y, f_z,)}{\widetilde{I}_\lambda(0,0)}, \tag{6}$$

where $\tilde{I}_\lambda$ (f_y and f_z) is the Fourier transform of the monochromatic brightness distribution projected on the sky, $I_\lambda(y, z)$, and f_y and f_z are the spatial frequencies in Fourier space defined by

$$f = \frac{B_{\rm proj}}{\lambda} \tag{7}$$

where $B_{\rm proj}$ is the baseline projected on the sky (Chesneau and Rivinius, 2005). The rotation of the Earth changes the projected baseline on the sky allowing different spatial frequencies to be observed. This is called (u, v) plane coverage (Stee et al., 2005).

An interferometer consists of: (1) at least two telescopes, and they should be of the same type with their mirrors oriented the same way and have the same coatings; three or more telescopes are advantageous, however, as they introduce an additional constraint during the closure phase between pairs of telescopes; (2) delay lines which are responsible for compensating for the optical path difference which results when different parts of the wavefront fall on different telescopes at different times; and (3) beam combiners which are responsible for getting the beams from the telescopes close together in order for them to interfere.

When light beams interfere, the interference pattern creates fringes, and the contrast of the fringes determines the modulus of the visibility – see Eq. (5) (Schöller, 2003).

In the field of Be stars, interferometric observations can place strong constraints on models of the circumstellar disks

Table 2 Interferometric observations of α Ara and ζ Tau.

Star	Instrument	JD	Baseline (m)	λ (μm)	FWHM (mas)	Model[e]
α Ara	VLTI/MIDI[a]	2453840.65972	126.8	12	3.6 ± 1.8	UED
	VLTI/MIDI[a]	2453841.82569	129.6	12	6.0 ± 2.3	UED
	VLTI/MIDI[a]	2453924.67778	120.7	12	8.1 ± 0.6	UED
	VLTI/MIDI[a]	2453840.65972	126.8	8	2.7 ± 1.1	UED
	VLTI/MIDI[a]	2453841.82569	129.6	8	3.9 ± 1.4	UED
	VLTI/MIDI[a]	2453924.67778	120.7	8	5.5 ± 0.3	UED
	VLTI/AMBER[b]	2453728.86528	52.5	2.1	7.6 ± 1.4	UED
ζ Tau	VLTI/MIDI[a]	2454842.65	127.3	12	5.7 ± 2.2	UED
	VLTI/MIDI[a]	2454842.65	127.3	8	< 2.6	UED
	CHARA[c]	2452830.5	249	2.1	1.79 ± 0.07	GD
	CHARA[d]	2454417.0	248	1.7	1.662 ± 0.042	GD
	CHARA[d]	2454419.0	248	1.7	1.527 ± 0.045	GD
	CHARA[d]	2454423.8	331	1.7	1.410 ± 0.025	GD
	CHARA[d]	2454421.4	331	1.7	1.599 ± 0.036	GD
	CHARA[d]	2454736.9	331	1.7	1.633 ± 0.031	GD
	CHARA[d]	2454810.8	331	1.7	1.116 ± 0.061	GD
	CHARA[d]	2455145.9	331	1.7	2.057 ± 0.060	GD

References:
[a] Meilland et al. (2009).
[b] Meilland et al. (2007).
[c] Gies et al. (2007).
[d] Schaefer et al. (2010).
[e] UED, uniform elliptical disk; GD, Gaussian disk.

as we can compare the output of detailed numerical models (e.g. the Fourier transform of a synthetic Be star image) to interferometric visibilities (Tycner, 2011). These observations can also detect asymmetries in the disk to find over-density regions and provide information about the rotational velocity of the disk (Tycner, 2010). One of the most important results obtained through interferometric observation of Be stars was the detection of Keplerian motion of the disk of α Ara by Meilland et al. (2007).

Many Be star disks have been resolved using long-baseline interferometry at IR wavelengths, and apparent disk sizes for the stars have been measured at different wavelengths (Gies et al., 2007; Meilland et al., 2008, 2009; Schaefer et al., 2010). For a stable disk, we expect that a unique disk density model (ρ, n and R_d) should be able to explain the observed change in the disk size with wavelength. Next, we review the observations and fitted disk sizes for the two well-studied Be stars, ζ Tau and α Ara.

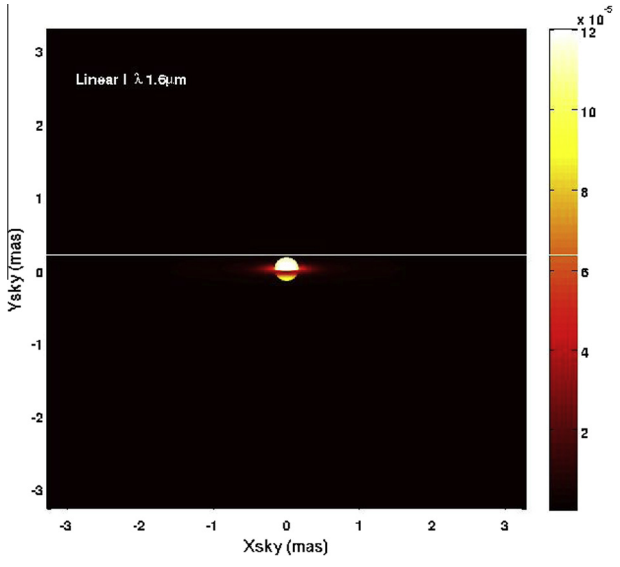

Fig. 1 Theoretical image of ζ Tau at $\lambda = 1.6$ μm constructed using BERAY, with the star parameters: B3V, $T_{\rm eff} = 18{,}000$ K and disk parameters: $\rho_o = 5 \times 10^{-11}$ g cm^{-3}, $n = 3$, i = 80°, and $R_d = 20\ R_*$.

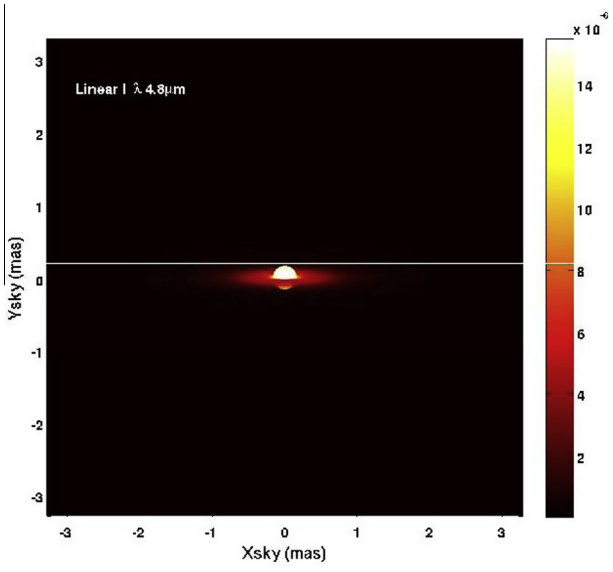

Fig. 2 Same as Fig. 1 but for $\lambda = 4.8$ μm.

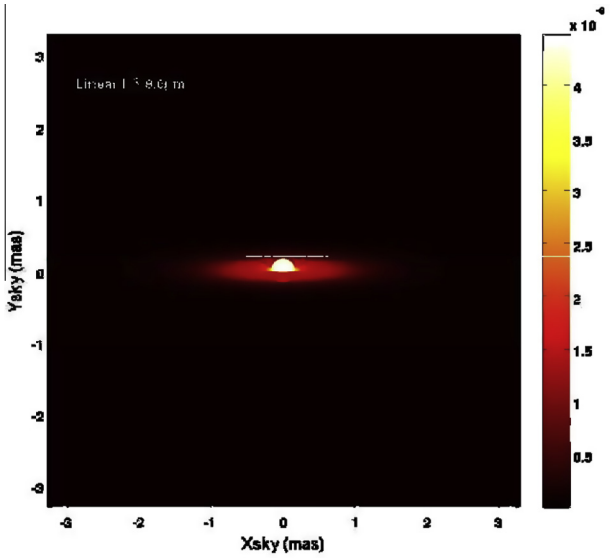

Fig. 3 Same as Fig. 1 but for $\lambda = 9$ μm.

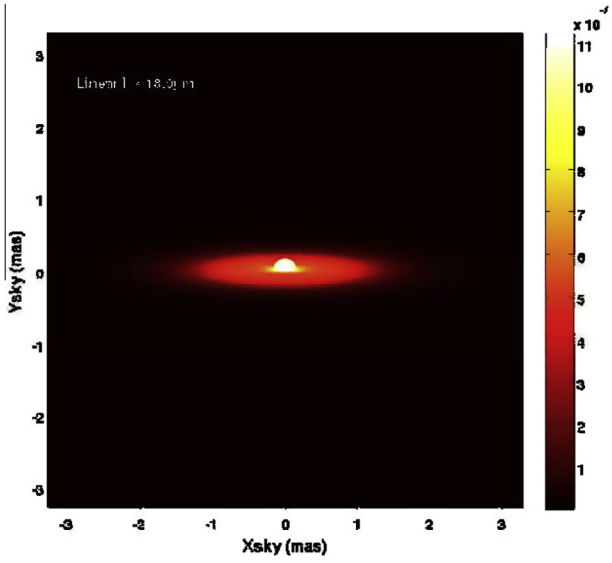

Fig. 4 Same as Fig. 1 but for $\lambda = 18$ μm.

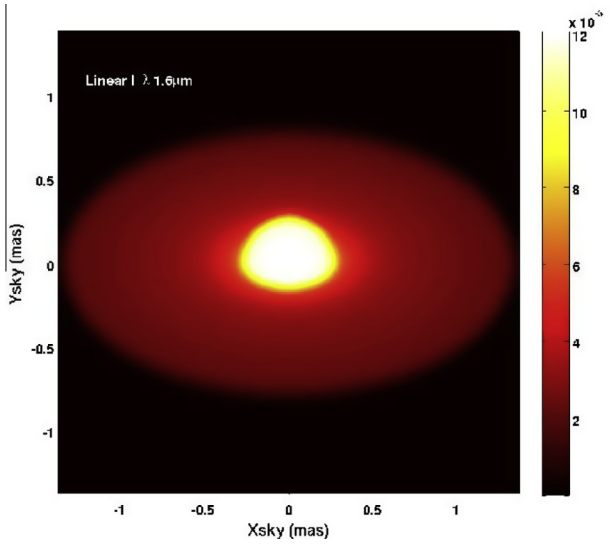

Fig. 5 Theoretical image of α Ara at $\lambda = 1.6$ μm constructed using BERAY with the star parameters: B3V, $T_{\rm eff} = 18{,}000$ K and disk parameters: $\rho_{\rm o} = 1 \times 10^{-10}$ g cm^{-3}, $n = 2$, $i = 55°$, and $R_d = 5\ R_*$.

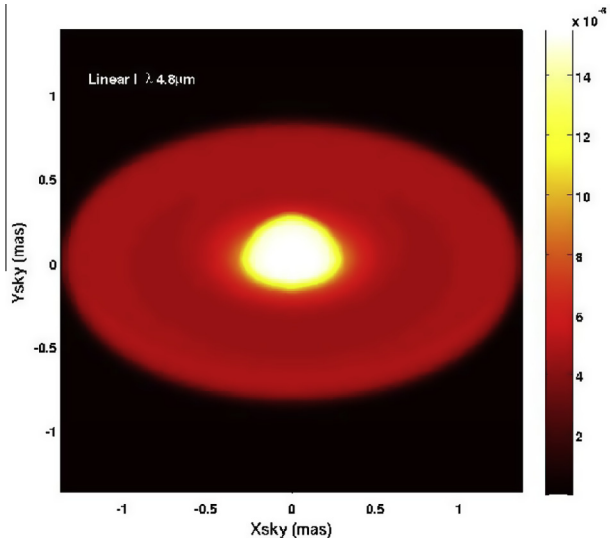

Fig. 6 Same as Fig. 5 but for $\lambda = 4.8$ μm.

3.2. ζ Tau

Tau (HR 1910, HD 37202, $V = 3.0$) is a Be star whose published luminosity class and spectral type are both uncertain (Schaefer et al., 2010). Estimates for the luminosity class of Tau range from III to V, and for its spectral class, from B2 to B4 (Meilland et al., 2009). We adopt a B3V model with $T_{\rm eff} = 18{,}000$ K, $R = 5.5\ R_*$, and $M = 11.2\ {\rm M}_\odot$. We also assume ζ Tau is viewed at an inclination angle 87° and lies at a distance of 136 pc (Quirrenbach et al., 1997; Meilland et al., 2009; Touhami et al., 2011). These stellar parameters are given in Table 1. It is believed that ζ Tau is a binary with a period of 132.91 days. The companion is a hot subdwarf with $T_{\rm eff} = 30{,}000$ K, $R = 1\ {\rm R}_\odot$, and $M = 1\ {\rm M}_\odot$ (Gies et al., 2007).

Gies et al. (2007) made K′-band ($\lambda = 2.1$ μm) long baseline interferometric observations for ζ Tau using the CHARA Array. The disk was resolved in their observations, and they calculated theoretical models for the star using the disk model of Hummel and Vrancken (2000). To do so, they solved the transfer equation to construct theoretical images of the star for different inclinations, base densities, and density exponents, assuming that the disk is isothermal with temperature $T_{\rm disk} = 0.6\ T_{\rm eff}$. They Fourier transformed these images to get the interferometric visibilities of the models, and they fitted the model disk parameters with the observed visibilities. They found a FWHM of 1.99 mas (milli-arcseconds) for a single B2IIIe star with a thick disk model. They also fit the K′ visibilities with a Gaussian ellipsoidal model getting a value of 1.79 ± 0.07 mas for the disk's FWHM.

Meilland et al. (2009) observed ζ Tau in the N band ($\lambda = 7.5$–14.5 μm) using VLTI/MIDI, and they fit a uniform

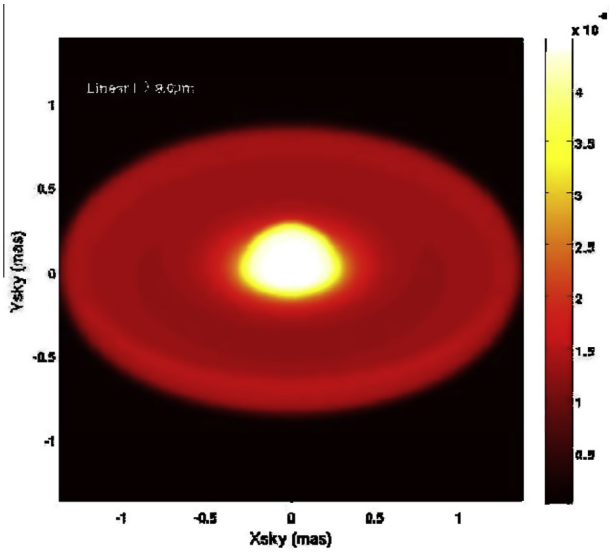

Fig. 7 Same as Fig. 5 but for $\lambda = 9$ μm.

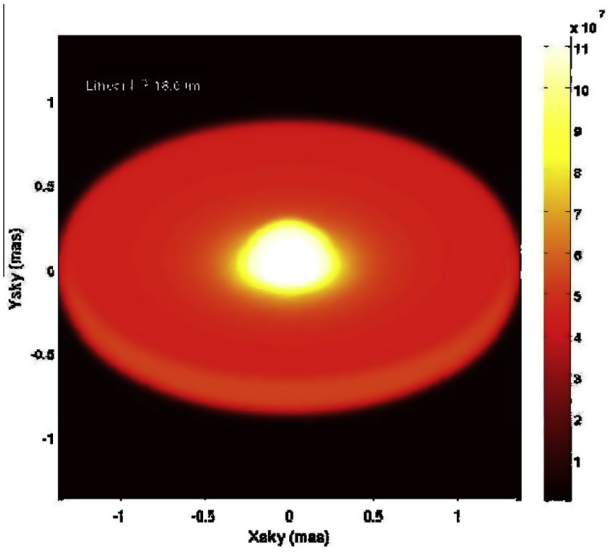

Fig. 8 Same as Fig. 5 but for $\lambda = 18$ μm.

disk for the circumstellar envelope. The disk was re-solved at $\lambda = 12$ μm where the length of the disk's major axis found to be 5.7 ± 2.2 mas. The disk was unresolved at $\lambda = 8$ μm so they put an upper limit on the length of the major axis of the disk of 2.6 mas.

Schaefer et al. (2010) used the MIRC beam combiner at the CHARA Array to perform multi-epoch interferometric observations for ζ Tau, and they were able to resolve the disk during four observational epochs. They fit a uniform disk for the central star and a skewed elliptical Gaussian for the disk to account for the asymmetry they detected in the closure phases. They modulated the Gaussian with a sinusoid as a function of the projected azimuth (or position angle) so that the brightness distribution of the disk will peak on one side and have a depression on the other. They found that the FWHM for the major axis of the disk ranges between 1.6 and 2.1 mas for different epochs, but they were unable to determine if this variation is due to a true change in the size of the disk. Touhami et al. (2011) adopted the weighted average of the disk FWHM in the H band ($\lambda = 1.7$ μm) to be 1.61 ± 0.05 mas. A summary of all available observations is presented in Table 2.

3.3. α Ara

α Ara (HD158 427, HR6510, $V = 2.9$) is a B3V star whose $T_{\rm eff} = 18{,}040$ K, $R = 4.8\ R_{\odot}$, $M = 9.6\ M_{\odot}$, and $d = 81$ pc (Chesneau et al., 2005; Meilland et al., 2009). These parameters can be found in Table 1. It has an unseen companion which is thought to have a mass ranging between 1.4 and 2.8 $M_{\odot}$, suggesting that its spectral type is F2-4V or A2-4V (Chesneau et al., 2005). Meilland et al. (2007) observed α Ara in the Brγ emission line and in the K-band continuum using the AMBER/VLTI instrument on February 23–24, 2005. Adopting a model for a B3Ve star, $T_{\rm eff} = 18{,}000$ K, $R = 4.8\ R_{\odot}$ whose angular size is equal to 0.7 mas, and assuming the system was viewed at $i = 45°$, they fit an unresolved star plus a uniform disk to the observations and find that the size of the disk in the K-band continuum is 7.3 ± 2 mas. Meilland et al. (2009) used VLTI/MIDI to make N band interferometric observations of α Ara, and they were able to resolve the circumstellar disk at $\lambda = 8$ μm and $\lambda = 12$ μm. They adopted a model for a B3V star and fitted a uniform disk finding a disk size of 5.8 ± 0.8 mas at $\lambda = 8$ μm and 8.2 ± 1.2 mas at $\lambda = 12$ μm. They noticed that the size of the disk does not vary significantly with increasing wavelengths, and they attribute this to a high-density disk truncated by a companion. A summary of the observations is presented in Table 2.

3.4. Calculations

The BEDISK code of Sigut and Jones (2007) was used to calculate the thermal and ionization structure for various disks surrounding ζ Tau and α Ara. The density distribution in the plane of the disk was assumed to be of the form $\rho(R) = \rho_{\rm o}(R_*/R)^n$. In the case of ζ Tau, we assumed it is a B3Ve star with $T_{\rm eff} = 18{,}000$ and calculated a range of models with the following parameters: base densities $\rho_{\rm o} = 1\times10^{-10}$, 1×10^{-11} and 5×10^{-11} g cm^{-3}; inclinations 70°, 80° and 87°; disk radii 10, 15 and 20 R_*; and power-law indices 2, 3 and 4. Then the BERAY code of Sigut (2011) was used to construct monochromatic images for these models on the sky for wavelengths ranging from 0.5 to 50 μm. BERAY solves the radiative transfer equation along a series of rays through the model and provides the monochromatic intensity at each grid point in the image. A Matlab code was then used to plot the theoretical monochromatic image on the sky. Example images for ζ Tau can be seen in Figs. 1–4.

A similar procedure was done in the case of α Ara where we assumed it to be a B3V star with $T_{\rm eff} = 18{,}000$. We made a range of models combining the following disk parameters: $n = 2$, 3 and 4; $\rho_{\rm o} = 1\times10^{-10}$, 1×10^{-11}, 2.5×10^{-11}, 5×10^{-11}, 7.5×10^{-11} g cm^{-3}; disk radii $R_{\rm d} = 5$, 10, 15 and 20 R_*; and inclination angles $i = 45°$, 55° and 75°. Examples for the theoretical monochromatic images of α Ara can be seen in Figs. 5–8.

To compare these models with the observations, we took horizontal cuts through the major axes of the images and fitted

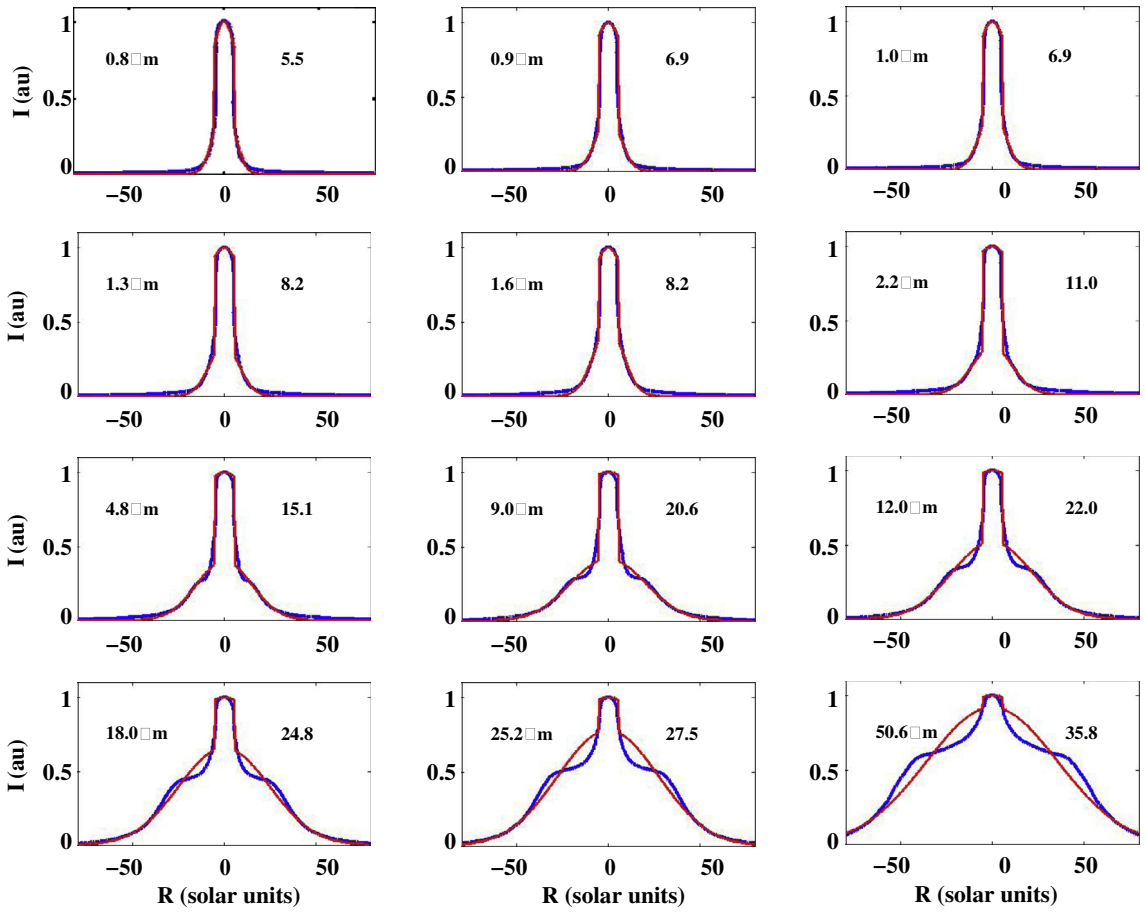

Fig. 9 Fitted models to the cuts along the major axis of the ζ Tau images (blue lines) and best fits for a star + a Gaussian disk (red lines) of Eqs. (8)–(10). The wavelength of each image (in μm) is shown to the left of each panel.

a uniform disk plus a Gaussian envelope to these cuts in the case of ζ Tau. The fitting function was taken to be

$$I(x) = \gamma I*(x) + (1-\gamma) I_D(x), \tag{8}$$

where

$$I_*(x) \begin{matrix} = I_o & if |x| \leqslant R_* \\ = 0 & \text{otherwise,} \end{matrix} \tag{9}$$

and

$$I_D(x) = e^{-x^2/\sigma^2} \tag{10}$$

Here I_o is the central star's photospheric intensity, I_D is the intensity of the disk, γ is a parameter giving the contrast between the star and the disk, and σ is the standard deviation of the Gaussian disk which is related to its size. As R_* and I_o are known, we fit for γ and σ. The FWHM of the Gaussian, 2.354 σ, was taken to be the the length of the disk's major axis (see Fig. 9).We did the same for α Ara, fitting a star plus a uniform elliptical disk to the cuts, taking the width of the ellipse as the length of the major axis of the disk (Fig. 10). In this case, we replaced Eq. (10) with

$$I_D(x) = \begin{matrix} I_D & \text{if } |x| \leqslant R_d \\ = 0 & \text{otherwise,} \end{matrix} \tag{11}$$

where R_d is the radius of the disk.

The Gaussian disk is the best model to describe a disk whose intensity is falling gradually outwards. Therefore we used it to model the disk of ζ Tau where we had a large disk whose intensity was falling toward the edges (see the blue lines in Fig. 9). In the case of α Ara, we have a small, dense disk with a uniform brightness distribution, and this is best modeled by a uniform disk (see the blue lines in Fig. 10).

3.5. Results

We used the observations of Table 2 to choose the best models to represent ζ Tau and α Ara by comparing the observed disk sizes with the theoretical ones at the available wavelengths. A Matlab code was used to process all the above mentioned models, taking the cuts through the major axis of the images and calculating the disk size as a function of wavelength using Eqs. (9)–(11). Then another Matlab code was used to choose the models that fit the observations best.

For ζ Tau, there were no models fitting all the observations; therefore, we chose models that fit the observations at 2.1 and 12 μm that were also quite close to the observations at 1.7 μm and the upper limit at 8 μm (see Fig. 11). The discrepancy between the models and the observations at these two wavelengths may be because of the variability of the star since the observations were taken at different epochs. All these best-fit

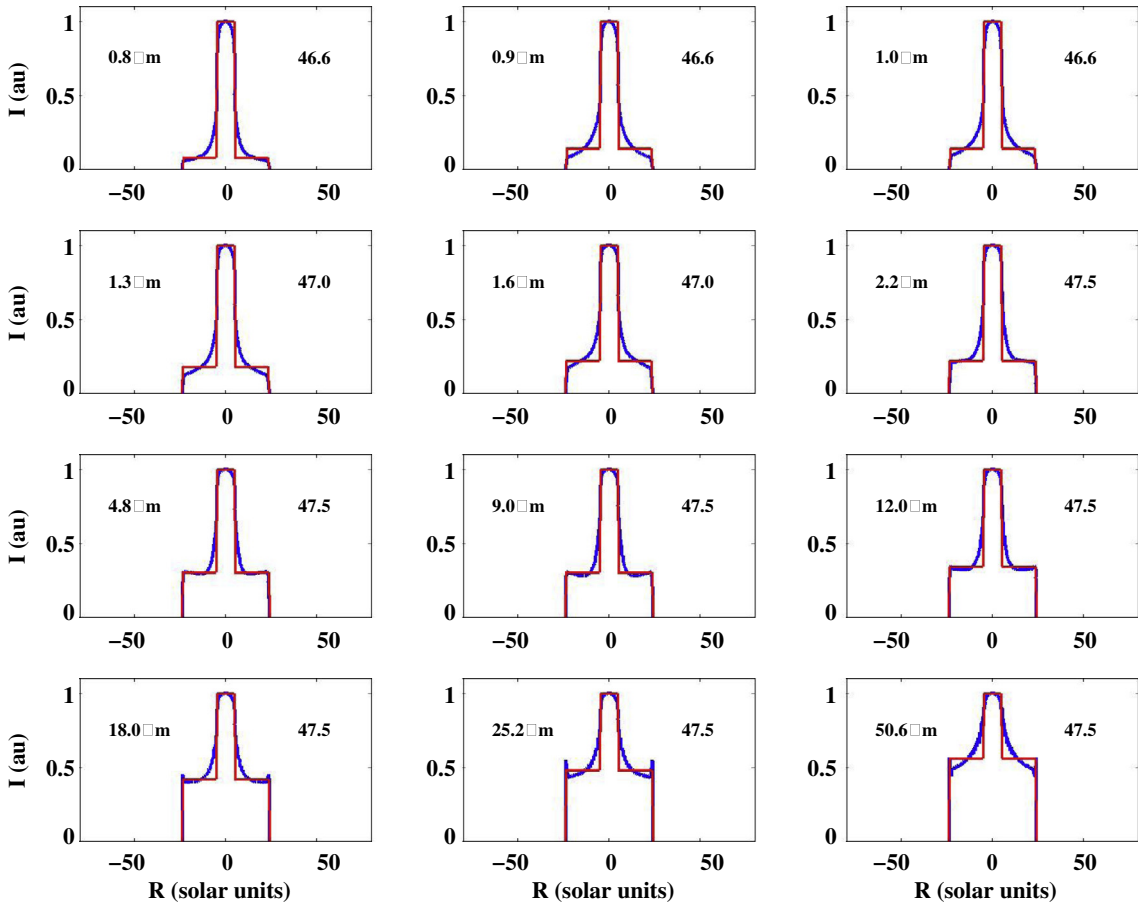

Fig. 10 Fitted models to the cuts along the major axis of the α Ara images (blue lines) and best fits for a star + a uniform elliptical disk (red lines) of Eqs. 8, 9, 11. The wavelength of each image (in μm) is shown to the left of each panel.

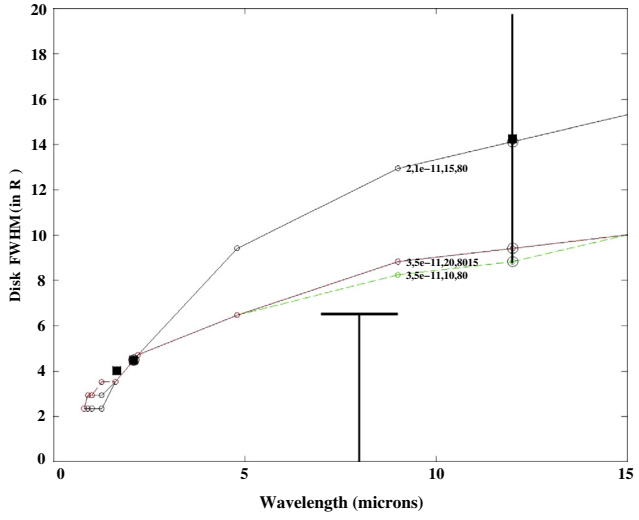

Fig. 11 Disk size as a function of wavelength for ζ Tau. Only the best models fitting are shown, and these models are listed Table 3. Here the disk FWHM is taken to be the width of the Gaussian component of the image fit. The lines are labeled by the model index (n), ρ, R_d, and inclination. Observational data are from Table 2.

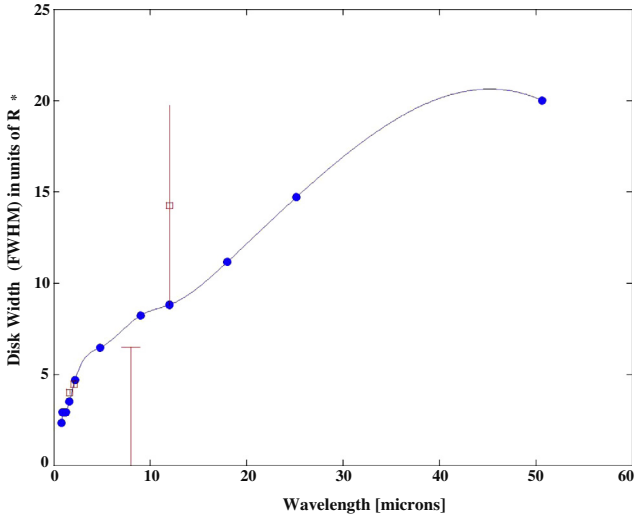

Fig. 12 FWHM as a function of wavelength for one of the models best fitting ζ Tau's disk. The model has the parameters $n = 3$, $\rho_o = 5 \times 10^{-11}$ g cm^{-3}, $R_d = 10\ R_*$ and $i = 80°$.

models were dense models with base densities of 1×10^{-11} and 5×10^{-11} g cm^{-3}; power-law indices of 2 and 3; and disk radii ranging from 10 to 20 R_*. All of them had an inclination angle

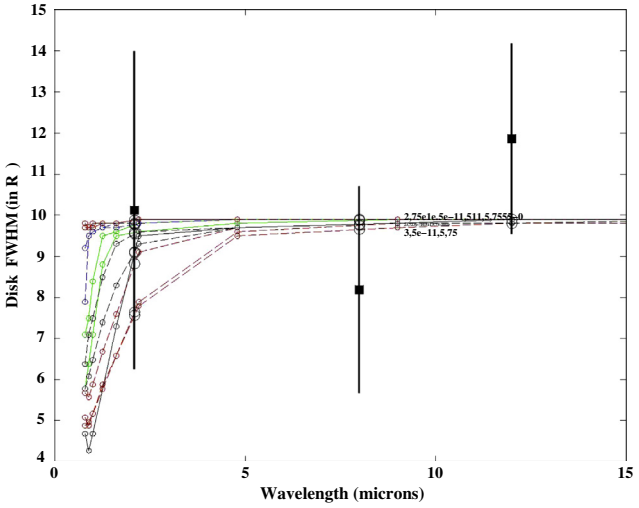

Fig. 13 Disk size as a function of wavelength for α Ara. Only the models fitting all the observations are plotted. These models are listed in Table 4. Here the disk's major axis is taken to be the width of the ellipse. The lines are labeled by the model index (n), ρ, R_d, and inclination. Observational data are from Table 2.

Table 3 Best models fitting ζ Tau. These models are shown in Fig. 11.

Power-law index	ρ_o (g cm^{-3})	Disk radius (R_*)	Inclination angle
2.0	1.0×10^{-11}	15.0	80
3.0	5.0×10^{-11}	15.0	80
3.0	5.0×10^{-11}	20.0	80
3.0	5.0×10^{-11}	10.0	80

Table 4 Best models fitting α Ara. These models are shown in Fig. 13.

Power-law index	ρ_o (g cm^{-3})	Disk radius (R_*)	Inclination angle
2.0	1.0×10^{-10}	5.0	55
2.0	1.0×10^{-10}	5.0	75
2.0	2.5×10^{-11}	5.0	55
2.0	2.5×10^{-11}	5.0	75
2.0	5.0×10^{-11}	5.0	55
2.0	5.0×10^{-11}	5.0	75
2.0	7.5×10^{-11}	5.0	55
2.0	7.5×10^{-11}	5.0	75
3.0	1.0×10^{-10}	5.0	55
3.0	1.0×10^{-10}	5.0	75
3.0	5.0×10^{-11}	5.0	75
3.0	7.5×10^{-11}	5.0	55
3.0	7.5×10^{-11}	5.0	75

of 80°. These models are summarized in Table 3.The model that was closest to all the observations had the parameters: $n = 3$, $\rho_o = 5\times10^{-11}$ g cm^{-3}, $R_d = 10\ R_*$, and $i = 80°$ (see Fig. 12). For all these models, the disk size showed a significant increase with wavelength as expected since the free–free opacity is proportional to the wavelength squared. This effect can be seen in Figs. 1–4.

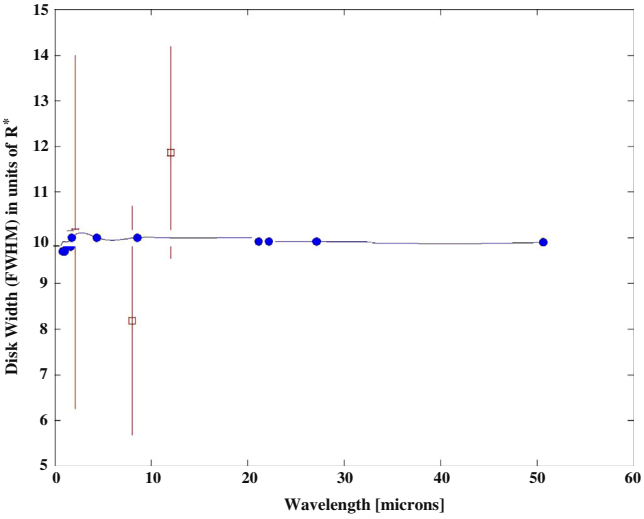

Fig. 14 Same as Fig. 12 for α Ara. The model has the parameters $n = 2$, $\rho_o = 1\times10^{-10}$ g cm^{-3}, $R_d = 5\ R_*$ and $i = 55°$.

There were 13 models fitting all the available observations for α Ara (see Fig. 13). All these models were for small, dense disks with disk radii of 5 R_* and base densities ranging from 2.5×10^{-11} to 1×10^{-10} g cm^{-3} and with power-law indices of 2 and 3, viewed at inclination angles of 55° and 75° (see Table 4). It can be seen from Fig. 13 that there is no significant increase in the size of the disk with increasing wavelengths. This can also be seen for the images for one of these models in Figs. 5–8. This is perhaps due to truncation by tidal interactions with a binary companion (Chesneau et al., 2005; Stee and Meilland, 2007; Meilland et al., 2007, 2009). In Fig. 14 we present an example of the disk size of α Ara as a function of wavelength with the disk parameters $n = 2$, $\rho_o = 1\times10^{-10}$ g cm^{-3}, $R_d = 5\ R_*$, and $i = 55°$.

4. Conclusions

We used the BEDISK and BERAY codes to construct theoretical images for the Be stars ζ Tau and α Ara projected on the plane of the sky. We calculated the sizes of the disks of these two stars and compared them with available interferometric observations. We found that the models best describing α Ara are dense, small disks, with a power-law index of 2 or 3, viewed at an inclination angle between 55° and 75°. These models were best fitted by a uniform disk because this dense disk had a uniform brightness distribution. The models we found to best fit ζ Tau's observations were for large disks with intermediate base densities viewed at an inclination angle of 80° with power-law index of 2 or 3. These disks were best described by a Gaussian disk model because the brightness distribution of this disk diminished toward the outer edge.

The lack of significant change in the observed size of the disk of α Ara between the 2.1 and the 12 μm may be explained by the dense, truncated disk model. The discrepancy between the model and the observations of ζ Tau at 1.7 and 8 μm may be attributed to the different epochs of observations at the four wavelengths and the lack of more available observations. More observations at different wavelengths are needed to further constrain the models.

References

Carciofi, A.C., Okazaki, A.T., Le Bouquin, J.-B., Stefl, S., Rivinius, T., Baade, D., Bjorkman, J.E., Hummel, C.A., 2009. Astronomy & Astrophysics 504, 915.

Chesneau, O. et al, 2005. Astronomy & Astrophysics 435, 275.

Chesneau, O., Rivinius, T., 2005. Publications of the Astronomical Institute of the Czechoslovak Academy of Sciences 93, 36.

Cranmer, S.R., 2005. The Astrophysical Journal 634, 585.

Gehrz, R.D., Hackwell, J.A., Jones, T.W., 1974. The Astrophysical Journal 191, 675.

Gies, D.R. et al, 2007. The Astrophysical Journal 654, 527.

Hummel, W., Vrancken, M., 2000. Astronomy & Astrophysics 359, 1075.

Maeder, A., Grebel, E.K., Mermilliod, J.-C., 1999. Astronomy & Astrophysics 346, 459.

Marlborough, J.M., 1969. The Astrophysical Journal 156, 135.

Meilland, A., Millour, F., Stee, P., Spang, A., Petrov, R., Bonneau, D., Perraut, K., Massi, F., 2008. Astronomy & Astrophysics 488, L67.

Meilland, A., Stee, P., Chesneau, O., Jones, C., 2009. Astronomy & Astrophysics 505, 687.

Meilland, A. et al, 2007. Astronomy & Astrophysics 464, 59.

Poeckert, R., Marlborough, J.M., 1978. The Astrophysical Journal 220, 940.

Porter, J.M., Rivinius, T., 2003. Publications – Astronomical Society of the Pacific 115, 1153.

Quirrenbach, A. et al, 1997. The Astrophysical Journal 479, 477.

Schaefer, G.H. et al, 2010. The Astronomical Journal 140, 1838.

Schöller, M., 2003. Memorie della Societa Astronomica Italiana Supplementi 2, 194.

Sigut, T.A.A., 2011. In: Neiner, C., Wade, G., Meynet, G., Peters, G. (Ed.), IAU Symposium, vol. 272, p. 426.

Sigut, T.A.A., Jones, C.E., 2007. The Astrophysical Journal 668, 481.

Stee, P., Meilland, A., 2007. In: Okazaki, S.S.A.T., Owocki, S.P. (Eds.), Astronomical Society of the Pacific Conference Series, vol. 361, Active OB-Stars: Laboratories for Stellar and Circumstellar Physics. p. 300.

Stee, P., Meilland, A., Berger, D., Gies, D., 2005. In: Ignace, R., Gayley, K.G. (Eds.), Astronomical Society of the Pacific Conference Series, vol. 337, The Nature and Evolution of Disks Around Hot Stars. p. 211.

Taylor, A.R., Waters, L.B.F.M., Lamers, H.J.G.L.M., Persi, P., Bjorkman, K.S., 1987. Monthly Notices of the Royal Astronomical Society 228, 811.

Touhami, Y., Gies, D.R., Schaefer, G.H., 2011. The Astrophysical Journal 729, 17.

Tycner, C. 2010. In: Revista Mexicana de Astronomia y Astrofisica Conference Series, vols. 27, 38, p. 81.

Tycner, C., 2011. In: Neiner, C., Wade, G., Meynet, G., Peters, G. (Eds.), IAU Symposium, vol. 272, p. 337.

Waters, L.B.F.M., 1986. Astronomy & Astrophysics 162, 121.

Woolf, N.J., Stein, W.A., Strittmatter, P.A., 1970. Astronomy & Astrophysics 9, 252.

Zorec, J., Briot, D., 1997. Astronomy & Astrophysics 318, 443.